Available online at www.sciencedirect.com
SCIENCE DIRECT®
Journal of Nuclear Materials 337–339 (2005) 781–785
journal of nuclear materials
www.elsevier.com/locate/jnucmat

Effect of B-field dependent particle drifts on ELM behavior in the DIII-D boundary plasma

M.E. Fenstermacher [a,*], A.W. Leonard [b], G.D. Porter [a], J.A. Boedo [c], N.H. Brooks [b], D.S. Gray [c], M. Groth [a], E.M. Hollmann [c], C.J. Lasnier [a], T.W. Petrie [b], L. Zeng [d]

[a] *Lawrence Livermore National Laboratory, Livermore, CA 94550, USA*
[b] *General Atomics, P.O. Box 85608, San Diego, CA 92186-5608, USA*
[c] *University of California at San Diego, La Jolla, CA 92093-0417, USA*
[d] *University of California, Los Angeles, CA 90095-1597, USA*

Abstract

Edge localized mode (ELM) effects in the DIII-D pedestal and boundary plasmas were measured with multiple fast diagnostics in matched, lower single-null, ELMing H-mode discharges with the ion $B \times \nabla B$ drift either toward or away from the divertor. Data show a strong dependence of the delay in inner vs. outer divertor ELM D_α on drift direction, and a weaker drift dependence of the inner vs. outer delay of P_{rad}, in addition to the strong density dependence seen in previous work. Time dependent boundary plasma modeling during an ELM was done with the UEDGE code including a six-species fluid carbon model and the effect of B-field induced particle drifts. The ELM was modeled as an instantaneous, outer midplane peaked, increase of diffusion coefficients from the top of the pedestal to the SOL. The simulations show delays in the inner vs. outer divertor ELM transients that are similar to the measured delays at moderate density.

PACS: 52.40.HF; 52.55.Fa; 52.65.−y; 52.70.−m
Keywords: ELM; DIII-D; SOL plasma boundary; Divertor modeling; Divertor plasma

1. Introduction

The interaction of transient particle and energy pulses with the plasma facing components (PFCs) during edge localized modes (ELMs) is a critical issue for the viability of future high power tokamaks. Projections for ITER indicate that the divertor target lifetime could be limited to $\sim 10^4$ unmitigated Type-I ELMs ($\sim$ several hundred full performance pulses) [1]. Finding operating regimes with good H-mode confinement and tolerable sized ELMs requires an understanding of both the ELM instability physics in the pedestal and the behavior of the transient pulses from ELMs in the boundary plasma.

This paper focuses on the effect of B-field dependent particle drifts on ELM behavior in the inner vs. the outer divertor of DIII-D as a function of plasma density.

* Corresponding author. Tel.: +1 858 455 4159; fax: +1 858 455 4156.
E-mail addresses: max.fenstermacher@gat.com, fenstermacher1@llnl.gov (M.E. Fenstermacher).

0022-3115/$ - see front matter © 2004 Elsevier B.V. All rights reserved.
doi:10.1016/j.jnucmat.2004.10.086

Previously the experimental variation, with plasma density, in the delay of the inner vs. the outer D_α emission transients during ELMs was found to be consistent with an ion convection model of scrape-off layer (SOL) ELM propagation [2,3]. This paper examines the effect of changing SOL and divertor particle drifts on the convection of ELM perturbations in the boundary plasma.

2. Description of experiments

For this study, lower single-null (LSN), H-mode plasmas with Type-I ELMs and matched input parameters and plasma shape were produced with the ion $B \times \nabla B$ drift direction toward (normal) and away from (reversed) the divertor by changing the direction of the toroidal field. Matched operational parameters included the plasma shape, toroidal field, $B_T = 1.75$ T, and plasma current $I_p = 1.2$ or 1.4 MA. A moderate triangularity, $\delta = 0.38$, moderate X-point height, $Z_{xpt} = 0.12$ m, shape was used to optimize the position of the divertor strike-points and X-point region for diagnostics. Some matched plasmas were obtained at both $q_{95} = 3.2$ (1.4 MA) and $q_{95} = 3.7$ (1.2 MA). Previous work with the normal drifts direction [2] had $q_{95} = 3.2$ (1.4 MA) and used a higher triangularity, $\delta = 0.52$. All available fast diagnostics [2] were set to simultaneously cover an overlap window of 500 ms during the flattop ELMing phase of the discharge, although many of the diagnostics obtained fast data beyond this overlap window.

3. Experimental results

Comparisons of coherently averaged ELM behavior from multiple diagnostics in matched moderate density ($n_e^{ped}/n_{Gr} \sim 0.35$) discharges with normal and reversed drifts show that the magnitude of the ELM effects are more similar and the transients more simultaneous in the inner and outer divertors for the reversed drifts case. The coherent averaging was done by aligning the data, in a time window about an ELM, to a time fiducial given by the peak of the D_α emission from the midplane tangential filterscope looking through the top of the pedestal. Results from matched normal (Fig. 1) and reversed (Fig. 2) drifts cases show that for the reversed drifts case, the increases in D_α and radiated power are more similar in the inner compared with the outer divertors and the evolution more coincident in time, than in the normal drifts case.

The D_α emission transients during ELMs in the inner divertor are delayed with respect to the outer divertor and the delay is larger in the normal drifts cases compared to the reversed drifts discharges. The delays, normalized to the difference in ion transit time from the outer midplane to the two divertors, $t_{transit}$, are shown

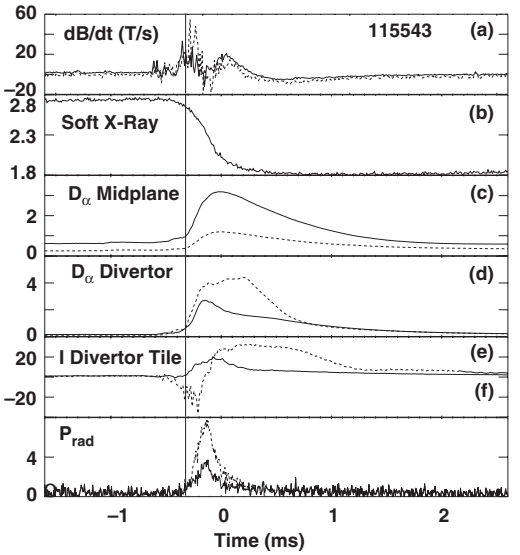

Fig. 1. Average ELM behavior in a normal drift discharge at moderate density, $n_e^{ped}/n_{Gr} = 0.35$ for (a) inner (---) and outer (—) divertor dB/dt (T/s), (b) pedestal soft X-ray signal, (c) pedestal (---) and midplane SOL (—) D_α, (d) inner (---) and outer (—) divertor D_α, (e) inner (---) and outer (—) strikepoint current (A) integrated on divertor tiles, (f) inner (---) and outer (—) divertor radiated power.

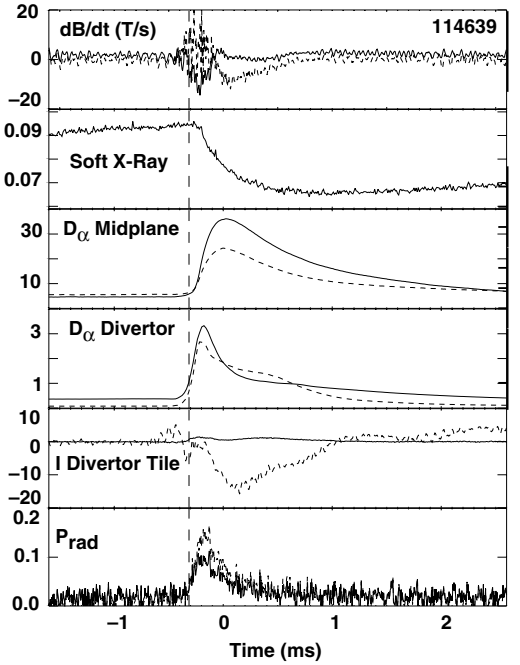

Fig. 2. Average ELM behavior in a reversed drift discharge at moderate density, $n_e^{ped}/n_{Gr} = 0.35$. Curves are the same quantities defined in Fig. 1.

in Figs. 3 and 4. Here, $t_{transit} = \Delta L_c / C_s(T_e^{ped})$ where $\Delta L_c = L_c^{in} - L_c^{out}$, $L_c^{in(out)}$ are the connection lengths between the outer midplane and the ISP (OSP) along the SOL field line connecting the locations of the D_α view spots on the targets, and $C_s(T_e^{ped})$ is the ion sound speed evaluated at the pedestal electron temperature before the ELM onset. The delay was obtained by selecting D_α data in a time window about each ELM, cross correlating the selected data from inner and outer divertor viewing chords, and fitting a Gaussian to the correlation function to find the most probable delay time. As seen previously in higher δ plasmas [2], there is a clear delay [Fig. 3(a)] of the inner D_α compared with the outer D_α in the normal drifts discharges with moderate to high density, $0.35 < n_e^{ped}/n_{Gr} < 0.8$, and this delay scales with $t_{transit}$. The normalized delay becomes very small at low density,

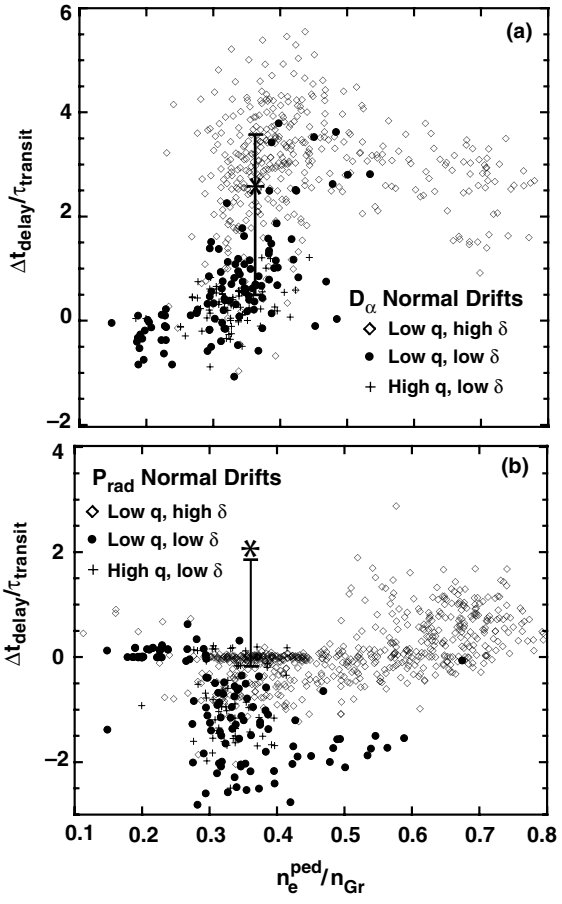

Fig. 3. Delay of inner vs. outer (a) D_α emission and (b) P_{rad}, normalized to transit time of ions at the pedestal energy, as a function of normalized pedestal density for the normal drift discharges. Range of delays from the simulations shown by vertical bar. Calculated delay on the flux tube corresponding to the measurements indicated by *.

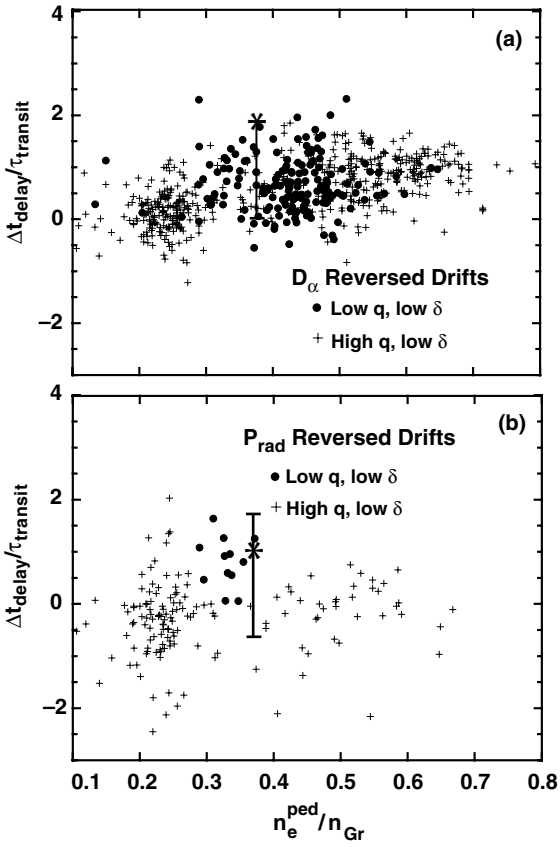

Fig. 4. Parameters of Fig. 3 for the reversed drift discharges.

$0.15 < n_e^{ped}/n_{Gr} < 0.30$. In the reversed drifts case [Fig. 4(a)], the normalized delay is a weakly increasing function of pedestal density, with much smaller delay at moderate to high density than in the normal drifts cases.

Very little delay is observed in the transient radiated power of the inner divertor compared with the outer divertor, independent of drifts direction; for many ELMs in the normal drifts case the local transient in the radiated power actually appears first in the inner divertor then in the outer divertor. Here the delay was obtained using the procedure described above applied to chords of the fast AXUV bolometer system [4]. In the normal drifts discharges, Fig. 3(b), positive delays (outer P_{rad} transients before inner P_{rad} transients) are observed in the high δ discharges at high density and small delays are observed at low density. P_{rad} transients in the lower δ discharges frequently appear first in the inner divertor (negative delay) for both the low and higher q_{95} plasmas. In the reversed drifts plasmas, Fig. 4(b), small delay is observed for most of the ELMs (albeit with significant scatter) in the higher q_{95} plasmas; the outer P_{rad} chord was saturated in most of the low q_{95} plasmas.

4. UEDGE modeling

Progress was made toward using the UEDGE multi-species fluid code [5] in time-dependent mode, with a 10× increase in transport coefficients for a short period, to simulate an ELM perturbation of the pedestal and SOL. The initial steady state H-mode solution prior to the ELM perturbation included a fluid neutrals model, all six charges states of carbon in a fluid impurities model and particle drift effects [6]. Neutrals in the model are assumed to be equilibrated by charge-exchange with the local T_i and carbon sources from physical and chemical sputtering are calculated from the Davis–Haasz model [7]. The drift effects include ion $B \times \nabla B$ and $E \times B$ drifts, but in these initial simulations the magnitude of the drifts was set to 40% of the full value predicted by theory. Guided by the average ELM behavior of Fig. 1 and Ref. [2], the ELM perturbation was modeled by an instantaneous 10× increase in the particle diffusion coefficient for 550 μs. For the last 50 μs of this period the energy transport coefficients were also increased by 10× over the steady state values. The perturbation was applied with a parabolic profile across the radius from the top of the pedestal to the outer SOL, and with a Gaussian poloidal profile peaked at the outer midplane with an e-folding poloidal length of 80 cm. ELM simulations for this study were based on steady-state UEDGE solutions for ELMing H-mode plasmas that had $\delta = 0.76$, $Z_{xpt} = 0.24$ m and $q_{95} = 4.0$, comparable to the high δ, Z_{xpt} discharges in the ELM characterization study. This shape was used because the higher δ and Z_{xpt} allowed UEDGE steady-state and ELM perturbation simulations to be obtained with the largest fraction of the theoretical drift effects included.

Simulations of chord-integrated D_α and radiated power signals, generated from the UEDGE time dependent simulations at $n_e^{ped}/n_{Gr} = 0.37$, showed positively correlated delay of the inner divertor signals relative to the outer divertor signals in the normal drifts cases and small delay of the inner vs. outer radiated power in the reversed drifts case, in qualitative agreement with experimental data at moderate density. The simulated chordal D_α and P_{rad} signals were calculated by integrating through the UEDGE 2D solution from the experimental diagnostic observation point to each of the target plate segments of the UEDGE solution. Positive

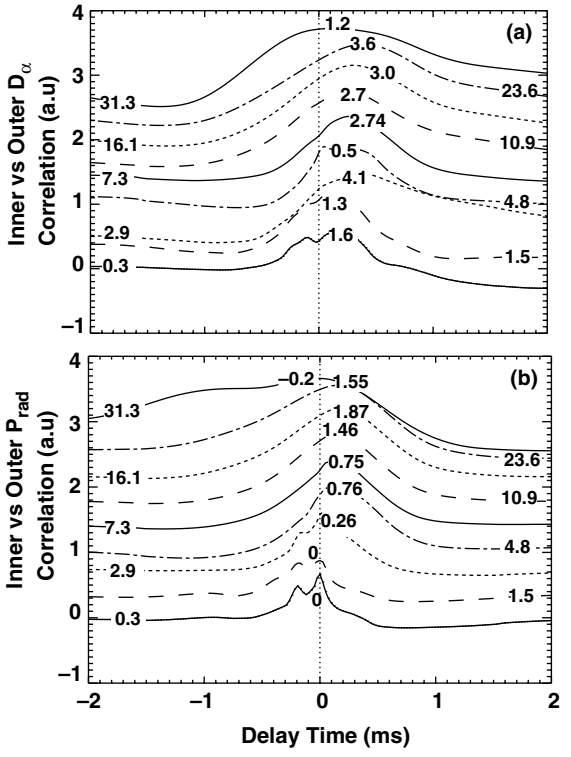

Fig. 5. Correlation probability as a function of inner vs. outer delay time of (a) D_α emission and (b) P_{rad}, for the normal drift UEDGE simulation. Correlation is done for locations on the inner and outer divertor targets that are on the same SOL flux surface. The midplane displacement of each flux surface from the separatrix (mm) is shown at the left and right. The most probable normalized delay for each flux surface is labeled near the peak of each correlation curve.

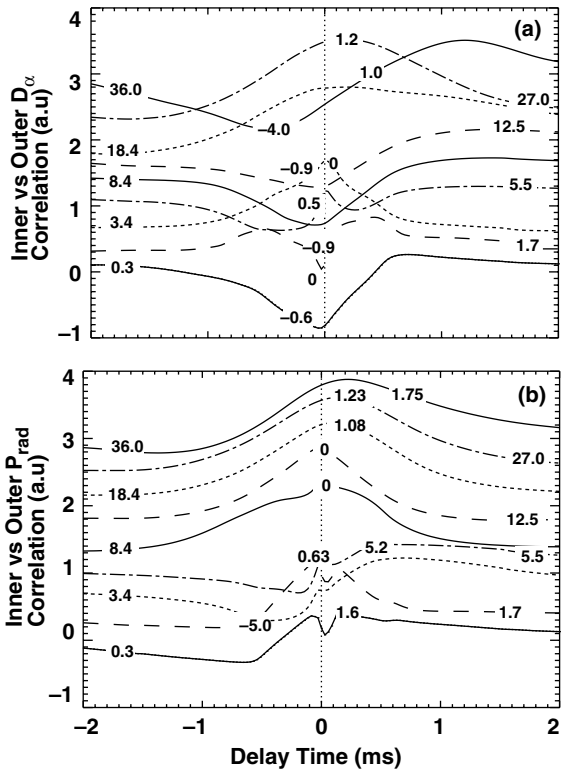

Fig. 6. Parameters of Fig. 5 for the reversed drift UEDGE simulation.

correlation (both signals increasing during the ELM transient) is predicted for the normal drifts case [Fig. 5] with larger in-out delays of D_α than of P_{rad}. This is consistent with the D_α data at moderate density in Fig. 3(a), but the negative delay of P_{rad} seen in the data is not reproduced. Positive correlation of P_{rad} is also calculated in the reversed drifts case [Fig. 6(b)] with small in-out delay similar to the data in Fig. 4(b). However, the UEDGE solution produces a mixture of positive and anti-correlation (one signal increasing and one decreasing during the ELM) in D_α at different SOL flux tubes between the inner and outer divertor in the reversed drifts case, Fig. 6(a). The positively correlated delays are consistent with the data in Fig. 4(a), but anti-correlation is not seen in the data.

5. Discussion and summary

The significant differences in the SOL and divertor behavior of ELM transients for LSN plasmas with normal and reversed drifts may be due to either differences in the pre-ELM condition of the SOL and divertor plasmas, or to the effect of the change in drifts direction during the ELM transient itself. For moderate pedestal density, the pre-ELM conditions in the normal drifts case include a cold, high density, detached inner divertor and a hot attached outer divertor. In contrast both divertors are attached in the reversed drifts case. The delays of both the D_α and P_{rad} transients between the inner and outer divertors are more sensitive to operating density in the normal drifts case. This may be due in part to the unbalanced conditions of the divertor legs before the ELM perturbation arrives, in particular the sensitivity of the inner leg detachment to operating density. D_α and P_{rad} transients occur nearly simultaneously in the two attached divertor legs for the reversed drifts case. Initial UEDGE modeling of D_α and P_{rad} transients during ELMs, with the effect of drifts included but in a slightly different plasma shape than the measurements, shows inner vs. outer delays in the normal drifts case comparable with the measurements. Anti-correlated transients, that are not seen experimentally, are calculated for the reversed drifts case. Future modeling will focus on better benchmarking to the pre-ELM conditions including plasma shape, incorporating the full theoretical drifts and developing a more realistic model of the ELM perturbation.

Acknowledgments

Work supported by US Department of Energy under W-7405-ENG-48, DE-FG02-04ER54758, DE-FC02-04ER54698, DE-AC05-00OR22725, DE-AC04-94AL85000, and DE-FG03-01ER54615.

References

[1] G. Federici et al., J. Nucl. Mater. 313–316 (2003) 11.
[2] M.E. Fenstermacher et al., Plasma Phys. Control. Fus. 45 (2003) 1597.
[3] M.E. Fenstermacher et al., in: Proc. 30th EPS Conf. on Plasma Phys. and Control. Fusion, St. Petersburg, Russia, 2003.
[4] D.S. Gray, S.C. Luckhardt, et al., Rev. Sci. Instrum. 75 (2004) 376.
[5] T.D. Rognlien et al., J. Nucl. Mater. 196–198 (1992) 80.
[6] T.D. Rognlien et al., J. Nucl. Mater. 313–316 (2003) 1000.
[7] J.W. Davis, A.A. Haasz, J. Nucl. Mater. 241–243 (1997) 37.